TECHNICAL PAPER

ISSN 1047-3289 *J. Air & Waste Manage. Assoc.* 50:357-370

Tomographic Reconstruction of Tracer Gas Concentration Profiles in a Room with the Use of a Single OP-FTIR and Two Iterative Algorithms: ART and PWLS

Doo Y. Park
Hansung University, Seoul, Korea

Jeffrey A. Fessler
University of Michigan, Ann Arbor, Michigan

Michael G. Yost
University of Washington, Seattle, Washington

Steven P. Levine
University of Michigan, Ann Arbor, Michigan

ABSTRACT

Computed tomographic (CT) reconstructions of air contaminant concentration fields were conducted in a room-sized chamber employing a single open-path Fourier transform infrared (OP-FTIR) instrument and a combination of 52 flat mirrors and 4 retroreflectors. A total of 56 beam path data were repeatedly collected for around 1 hr while maintaining a stable concentration gradient. The plane of the room was divided into 195 pixels (13 × 15) for reconstruction.

The algebraic reconstruction technique (ART) failed to reconstruct the original concentration gradient patterns for most cases. These poor results were caused by the "highly underdetermined condition" in which the number of unknown values (156 pixels) exceeds that of known data (56 path integral concentrations) in the experimental setting. A new CT algorithm, called the penalized weighted least-squares (PWLS), was applied to remedy this condition. The peak locations were correctly positioned in the PWLS-CT reconstructions. A notable feature of the PWLS-CT reconstructions was a significant reduction of highly irregular noise peaks found in the ART-CT reconstructions. However, the peak heights were slightly reduced in the PWLS-CT reconstructions due to the nature of the PWLS algorithm. PWLS could converge on the original concentration gradient even when a fairly high error was embedded into some experimentally measured path integral concentrations.

It was also found in the simulation tests that the PWLS algorithm was very robust with respect to random errors in the path integral concentrations. This beam geometry and the use of a single OP-FTIR scanning system, in combination with the PWLS algorithm, is a system applicable to both environmental and industrial settings.

IMPLICATIONS

Gas concentration mapping in a room-sized chamber with the use of CT techniques, coupled with OP-FTIR, demonstrates that this system and reconstruction method could be directly applied in many environmental and industrial settings. The experimental beam configuration was in the highly underdetermined condition, which is commonly encountered in most conceivable fields. A new CT algorithm, the PWLS, was applied to remedy this unfavorable condition, since the standard ART algorithm results in poor CT reconstructions. Generally, concentration gradient patterns and peak locations were successfully reproduced. This system is the first experimental verification for the practical application of a CT system for real air pollutant mapping.

INTRODUCTION

Computed tomography (CT) coupled with optical remote sensing has recently been introduced to measure the spatial distribution of gas and vapor pollutant concentrations in environmental, indoor, and workplace air monitoring.[1-6] The potential advantages of this technique have been extensively discussed in the literature.[3,7-11] In early papers on the subject, CT methods were conceptually shown to have the potential for good reconstruction

of air pollutant concentrations in a plane under certain narrowly limited conditions.[3-6]

Recently, experiments by our group have successfully demonstrated CT reconstructions in a room-sized chamber.[8-10] The first experimental study on the CT reconstruction of indoor air concentrations, coupled with open-path Fourier transform infrared (OP-FTIR) spectrometers, was reported by Yost et al.[8] The experiments were conducted with the use of a single bi-static OP-FTIR. Thus, the source and detector had to be moved substantially to get the desired sets of parallel rays. Parallel ray data with four projection angles were obtained. However, long measurement times were necessary to scan the whole plane.

The follow-up experimental tests were conducted by using a single OP-FTIR capable of rapid beam movement by the computer-controlled steerable mirror in a pilot scale-chamber, which allowed us to significantly reduce measurement times to scan the whole plane. One of the simplest beam configurations was selected for the experiment, based on the numerous computer simulation tests that have been reported by Park et al.[11] However, extremely poor CT reconstruction results were obtained from the original experimental tests, because of an insufficient number of rays and projection angles. In theoretical study, it has been shown that more complicated beam configurations are apparently able to produce good CT reconstructions as demonstrated.[11] However, when working with more complicated beam configurations, a cost problem will accompany a greater number of rays and projection angles.

Besides the configuration of the beam geometry, the CT algorithm is also a major determinant for the quality of CT reconstructions. Again, poor CT reconstructions resulted from a "highly underdetermined condition," that the number of unknown values (156 pixels) exceeds that of known data (56 path integral concentrations) in the experimental setting. In this condition, the CT reconstructions with the algebraic reconstruction technique (ART) were not satisfactory because the rays in the experimental geometry were less independent. A great deal of effort was expended to solve this problem by using new CT methods along with realistic ray configurations.

Drescher et al. reported a new CT method, smooth basis function minimization (SBFM), to overcome the limitations of ART.[9] Much improvement in the quality of CT reconstructions was achieved by applying the SBFM to the experimental data, compared to those applied with ART.[9,10]

Another effort was made to remedy uncertainty resulting from the highly underdetermined condition by applying a penalized weighted least-squares (PWLS) image reconstruction method. The PWLS method was originally developed by Fessler for positron emission tomography (PET).[12,13] This paper reports how PWLS could effectively reduce unrealistically high noise levels of the CT reconstructions which were found when using ART. Six experimental results in a room-sized chamber and simulation tests demonstrate that this system and reconstruction method could be directly applied in many environmental and industrial settings.

EXPERIMENTAL DESIGN AND METHODS

Experimental Chamber

The chamber was designed to provide stationary dilution ventilation to maintain stable air pollutant concentration patterns. The chamber was built with a wooden frame covered by a thick polyethylene liner, and was inside a large building to minimize the influence of turbulence caused by outside wind. The dimensions of the chamber were $6.4 \times 7.3 \times 2.4$ m^3 (Figure 1). Air was driven through a 6.4×0.92 m^2 slot in the ceiling along one side of the wall of the chamber. This slot was connected to a large fume hood that allowed adjustment of the air flow rate from about 28 to 113 m^3/min (1000 to 4000 cfm). Two 6.4×0.46 m^2 slots were installed at one of the short walls to supply fresh air. A 6.4×0.92 m^2 slot was installed at

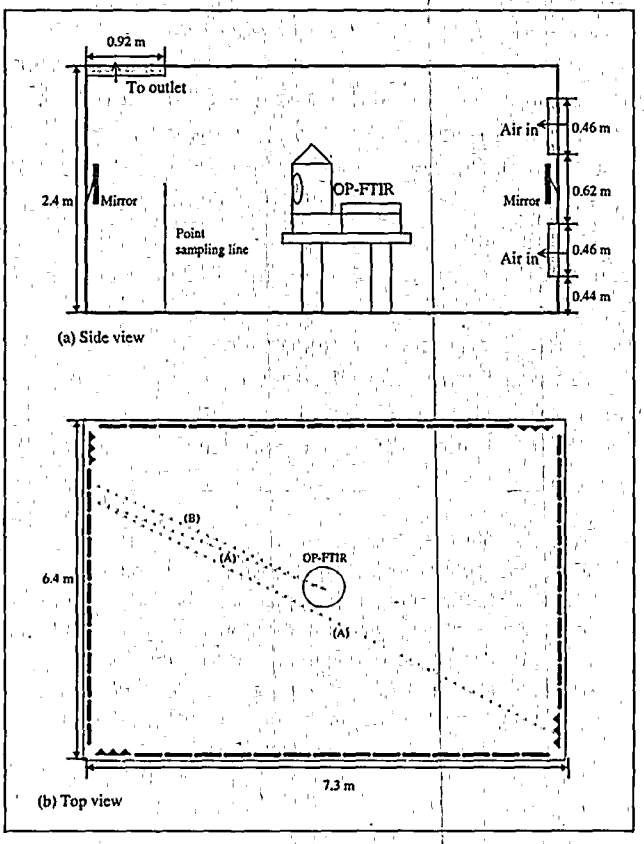

Figure 1. Schematic of the experimental chamber. (a) Side view. OP-FTIR was located at the center. Thirty-one point samples were taken on a horizontal plane at the center of the beam paths. (b) Top view. One retroreflector was placed at each corner and 52 flat mirrors were installed along the perimeter of the walls. Dotted lines show examples of a folded ray (A) and a short ray (B).

the ceiling along the opposite side of the chamber. All slots were covered with coarse-fibered, 2.5-cm-thick furnace filter material to provide a uniform air flow.

A mixture of 10% sulfur hexafluoride (SF_6) in helium was used as a tracer gas in this study. SF_6 was released at a constant emission rate through a 2.5-cm-diameter, porous ceramic sphere at a height of 0.6 m from the floor. The emission rate was controlled with the use of a needle valve. Flow rate was measured by a rotameter calibrated with a bubble meter. Various concentration gradient profiles were obtained from different arrangements of emission sources, locations, and flowrates.

All operations for running the OP-FTIR scanning system were remotely conducted from outside the chamber with the use of a remote computer. Air bag samples were also collected from outside the chamber using Teflon tubing.

OP-FTIR Scanning System

Path integral concentrations (concentration × path-length in meters) were measured with the use of an OP-FTIR scanning system (MDA Scientific Inc., now ETG Inc.). This system was designed as a monostatic unit that uses a single transmitter/receiver telescope. The infrared radiation was modulated by a Michelson interferometer, of a wishbone design, which uses corner-cube retroreflectors. The modulated infrared radiation is collimated by a 20-cm-diameter Cassegrain telescope and transmitted through the atmosphere to a retroreflector, which reflects the beam back to the telescope. The radiation is then focused on the aperture of a liquid-nitrogen-cooled mercury-cadmium-telluride (MCT) detector. An IBM-compatible 486 PC was connected for data collection and spectral analyses. The recorded signal in the form of an interferogram was Fourier-transformed to produce a spectrum from 700 to 4500 cm^{-1}, with 1 cm^{-1} resolution using the MDA continuous monitor software package (ETG Inc.). Approximately 4.5 sec were required to collect one-path integral concentration with a single spectral scan.

A self-contained beam aiming device that allows translation of the beam in the horizontal and vertical axes was installed in the front of the telescope. The computer-controlled solenoid permits beam slewing rates of 10 degrees/sec. The beam aiming parameters were trained into the PC-based data system. Through the use of this device, 56 path integral concentrations were measured sequentially in the same direction during the experiment.

Quantitative spectral analyses for SF_6 concentrations were performed with the use of a classical least-squares fit program (MDA continuous monitor software package, ETG Inc.). For each experiment, the clean air background spectrum for each ray was collected before releasing SF_6. Quantitation was conducted in a spectral window at 917–975 cm^{-1} using a reference spectrum of 66 ppm-m SF_6, which was provided in the MDA continuous monitor software package.

Beam Configuration

This study used a single OP-FTIR scanning system, 52 flat mirrors, and 4 retroreflectors. A network of intersected beam paths was obtained by a combination of 52 flat mirrors and 4 retroreflectors using a single OP-FTIR. Four retroreflectors for returning the beam back to the flat mirrors and OP-FTIR were used instead of flat mirrors because it was extremely difficult to align the beam using two flat mirrors. Fifty-two aluminum coated mirrors (254 × 313 mm^2, Part # M32248 Edmund Scientific Co.) were installed along the perimeter of the chamber. Only four retroreflectors were used in this study because using corner cube retroreflector arrays is quite expensive. A 35 × 35 cm^2 corner cube retroreflector array (ETG Inc.) was placed at each of the four corners of the chamber (Figure 2).

The OP-FTIR scanning system was located at the center of the chamber. Not all flat mirrors could redirect the beam to the retroreflectors at the opposite side. Fourteen flat mirrors were placed along each long side, but only 13 of these mirrors could be used to obtain folded beams. Enough radiation signal strength for quantitative analysis could not be measured when the 14th flat mirror was used to redirect the beam to the retroreflectors. This was due to limitation of the retroreflectors, which can reflect the beam to the origin only within a limited angle of 24° from the center line. Therefore, these beam paths were measured only from the OP-FTIR to the flat mirrors. Also, the 12th flat mirror along the short side could not generate the folded beam because the OP-FTIR located at the center blocked the beam. These beam paths were also measured just from the OP-FTIR to the flat mirrors. In addition, four short rays were measured from the OP-FTIR to four retroreflectors. Thus, a total of 56 path integral concentrations were measured for the whole plane of the chamber. During alignment of every beam path for each experiment, the signal detection of the FTIR was checked to confirm that the beam was not traveling to adjacent mirrors by blocking the target mirror with a white paper.

Approximately 6 min were taken to scan the whole plane of 56 path integral concentrations. Each experiment was conducted for 1 ~ 1.5 hr. Nine to 14 replication sets for the whole plane of all 56 rays were collected during each experiment.

The pixel size was set as 0.49 × 0.49 m^2, based on consideration of the beam width and size of the flat mirrors and retroreflectors. It was also considered that this pixel size could represent a worker's breathing zone. The horizontal measurement plane was divided into a 13 × 15 grid

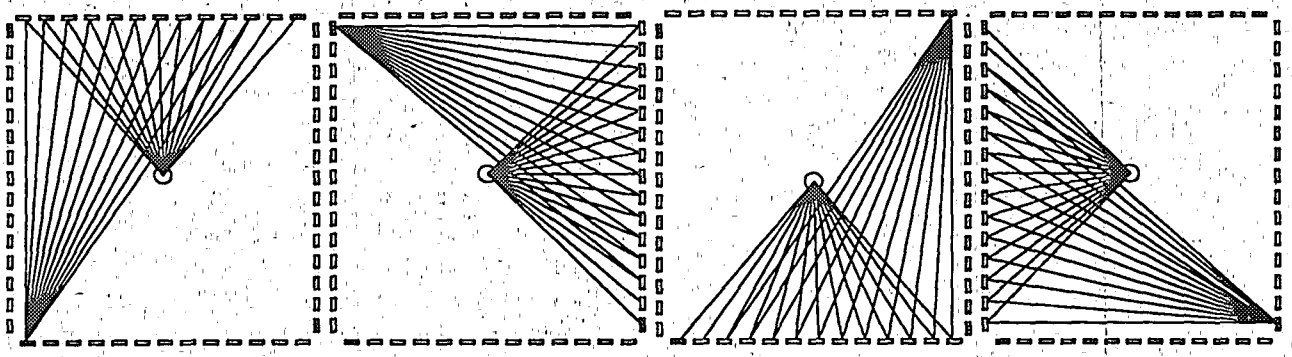

(a)

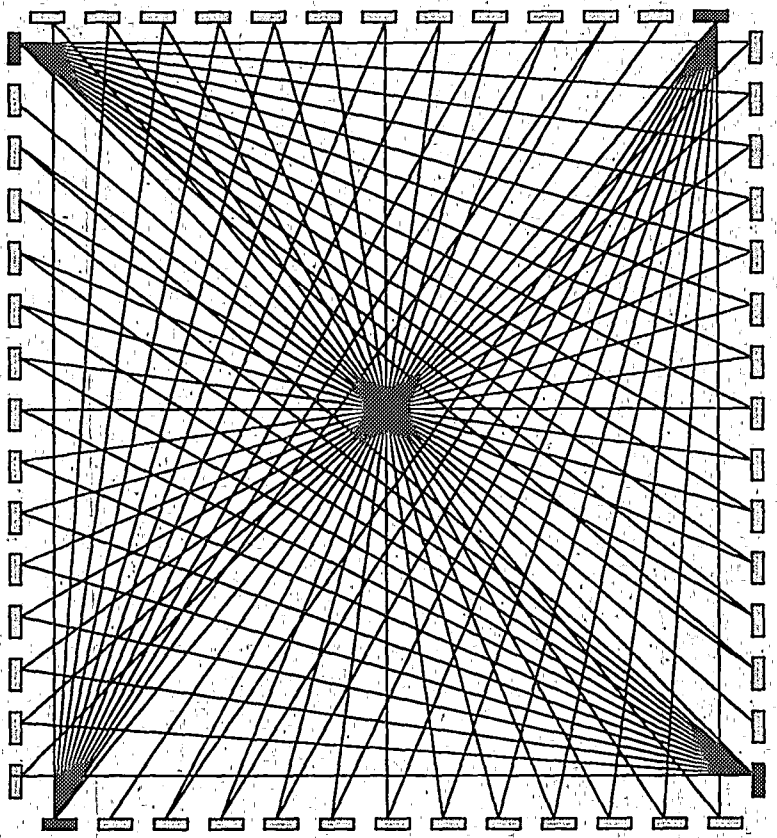

(b)

Figure 2. Schematic representation of beam configuration with 52 flat mirrors and 4 retroreflectors at the chamber perimeter. An OP-FTIR scanning system is placed at the center. Forty-eight folded ray integrals and eight short rays could be obtained. (a) View of each of four projection angles. (b) Total beam configuration. Gray rectangles represent flat mirrors, black rectangles represent retroreflectors.

map for CT reconstructions. Therefore, a total of 195 pixels were reconstructed.

Point Sampling

Time-integrated SF_6 concentrations at 31 point locations were measured during the collection of path integral concentrations. A photoacoustic infrared detector (Multi-Gas Monitor, Type 1302, Bruel & Kjaer Instruments) was used to analyze SF_6 concentrations. Air samples were taken from 31 points at the same height with the center of the beam paths in each experiment. Air from five sampling points was drawn continuously, at a flow rate of 1 L/min, through 2.3-L glass jars. Air samples were sequentially taken and analyzed once every 6 min by an automatic sampler (Multipoint Sampler, Type 1309, Bruel & Kjaer Instruments) and the photoacoustic detector. They were collected into gas sampling bags (12-L Tedlar bag, SKC Inc.) at 26 points, and SF_6 concentrations were subsequently analyzed using the photoacoustic detector. The photoacoustic detector was calibrated by using a standard gas of 50 parts per million (ppm) SF_6 in helium for each experiment.

Point sampling locations were mostly evenly distributed in a measurement plane. However, where steep concentration gradients were expected, denser point samples were taken. All point sample data were kriged into a 13 × 15 grid map to produce a two-dimensional concentration map over the measurement plane using the computer program SURFER (Golden Software).[14] Therefore, it was unavoidable to introduce a certain level of artifacts during the kriging interpolation for 195 pixel values from the 31 point samples. This became evident because the kriging interpolation resulted in negative values in some of the pixels. The negative pixel values were adjusted to zero after the kriging interpolation.

These kriged point sample data were used as the test maps for the simulation tests. For simulation tests, synthetic path integral concentrations were calculated, and these synthetic ray data were used for CT reconstruction processes.

Reconstruction Algorithms: ART and PWLS

Two iterative algorithms were applied for the CT reconstructions in this study: ART and PWLS. Iterative algorithms were chosen because of good flexibility for various beam configurations. The ART algorithm has been reported to work well with a limited number of path integral concentrations and projection angles. The ART algorithm iteratively adjusts the concentration in each pixel along the rays to minimize the differences between the measured path integral concentrations and the path integral concentrations calculated from the CT reconstruction. The ART algorithm is described in detail in the literature.[15]

The process of CT reconstruction using ART was implemented by using a program written in Turbo PASCAL (Borland). The initial concentration of each pixel was assigned as zero. During one iteration process, pixel concentrations were adjusted for all rays in the sequence by distribution of the difference between measured (true) and calculated path integral concentrations, so that the differences were minimized. The only additional constraint was that the pixel concentration should not be less than zero. Thus, negative pixel values were corrected to a value of zero at each iteration.

A value of σ_{ray} was used to indicate the overall agreement between the true path integral concentrations and the calculated path integral concentrations from a reconstructed concentration map after a given iteration. The σ_{ray} value was calculated as follows:

$$\sigma_{ray} = \sqrt{\frac{\sum_{i=1}^{n}\left(R_{true,\,i} - R_{recon,\,i}\right)^2}{\sum_{i=1}^{n} R_{true,\,i}^2}} \qquad (1)$$

where $R_{true,\,i}$ is the experimental or synthetic path integral concentration value of the ith ray. $R_{recon,\,i}$ is the calculated path integral concentration value of the kth ray from the CT reconstruction. A lower value of σ_{ray} indicates a better agreement between the average concentrations along the rays of the reconstruction and the true data (calculated from the original test map). For perfect agreement, σ_{ray} is zero. This has been explained in detail elsewhere.[9]

The σ_{ray} value was calculated and used for a stopping criteria for the iteration process. The reconstruction was terminated when the fractional change in σ_{ray} from one iteration to the next was less than 0.005. The fraction change was defined as follows:

$$\text{Fraction change} = \frac{\sigma_{ray,\,k+1} - \sigma_{ray,\,k}}{\sigma_{ray,\,k}} \qquad (2)$$

where $\sigma_{ray,\,k}$ and $\sigma_{ray,\,k+1}$ are the σ_{ray} values of the kth and $(k+1)$th iterations, respectively.

The PWLS image reconstruction method was applied for this study. PWLS is also an iterative reconstruction algorithm. Thus, it can be easily applied for the ray configurations for which projections are not uniformly distributed in a plane, and which have a limited number of rays and projections. In addition to the agreement between measured and calculated path integral concentrations, PWLS imposes an additional smoothness constraint that discourages disparities between neighboring pixel values.[12,13]

The effect of the penalty term is to discourage disparities between neighboring pixel values. Therefore, the PWLS algorithm increases agreement between the true (or measured) path integral concentrations and the calculated ones from the CT reconstruction, and decreases

discrepancies between adjacent pixel values during each CT reconstruction process. A weighting factor for the smoothing penalty, called a smoothing parameter (β), controls these two conflicting objectives. While the ART algorithm iterates to decrease only the σ_{ray} values, the PWLS algorithm iterates to decrease the σ_{ray} values and also to increase the smoothness of the reconstruction by incorporating a smoothing penalty.

The image smoothness increases as β increases. When β is extremely low, the PWLS algorithm will mainly force a match of the path integral concentrations. This is similar to the ART process. Therefore, the reconstructions using the PWLS algorithm with very low β value will be similar to those generated by ART.

It was necessary to balance weighting of the smoothing penalty to achieve the best reconstruction using the PWLS algorithm. However, there was no unique method to decide the optimal magnitude for β. The optimum value of β was dependent on both the concentration gradient patterns and the objectives of the CT reconstructions. If the general concentration gradient pattern was of greater importance than the concentration peaks, higher β values would be desirable. On the contrary, lower β values would be preferable for identifying pollutant leaks or emission sources. It is beyond the scope of this study to develop and investigate the method for selecting optimum β values for differing scenarios. It was concluded that the best reconstructions were achieved for these tests when the σ_{pixel} value was minimized; that is, the best reconstructions were determined based on the overall agreement between the true map and the CT reconstructions in this study.

CT reconstructions with PWLS were implemented by using a computer program written in ANSI C.[12] Various values for β were evaluated in the simulation tests. An appropriate smoothing parameter for each concentration gradient profile was estimated based on the empirical data.

Evaluation of the CT Reconstructions

There is no universal quantitative parameter with which to evaluate reconstruction quality in either simulation tests or field tests. Several quantitative terms and visual assessments have been developed and used to evaluate CT reconstructions.[2,4,10] However, it is extremely difficult to evaluate the CT reconstructions in most experimental or real field situations because the real concentration profiles are not exactly known.

A parameter σ_{pixel} was defined to quantify the overall agreement of the pixel concentrations between the CT reconstruction and the true map. This parameter is useful when the true concentration profile is known, and has thus been widely used in many simulation studies.[9-11] It is calculated as

$$\sigma_{pixel} = \sqrt{\frac{\sum_{p=1}^{n}\left(C_{p,\,test} - C_{p,\,recon}\right)^2}{\sum_{p=1}^{n} C_{p,\,test}^{\,2}}} \qquad (3)$$

where $C_{p,\,test}$ is the concentration in a pixel obtained from the true map (in the simulation test, the original test map) and $C_{p,recon}$ is the pixel concentration calculated from the reconstruction map. The σ_{pixel} value reflects the degree of matching between the pixel concentrations in the test map and reconstruction map. A lower value indicates better agreement between the CT reconstruction and the true map. The σ_{pixel} value is zero for a perfect match. However, it is a relative parameter rather than an absolute value for a given concentration gradient. Thus, it can be used to compare the degree of agreement of the CT reconstruction to the true map only for a given concentration profile (i.e., a value of the σ_{pixel} does not make comparisons between different concentration profiles).

The CT reconstructions were also compared visually to the kriged map of the point sample data. Visual assessment usually provides useful information for evaluation of peak heights, locations, smoothness, and artifacts of the reconstructions. For replications of the CT reconstructions in simulation tests with yhe introduction of random noise to synthetic path integral concentrations, the average of replications was visually evaluated, and the standard deviation as a function of pixel was plotted for evaluation.

The averages of all pixel values for CT reconstruction were compared with those of the kriged map from point sample data for evaluation of bias. The averages of path integral concentrations were also compared between the kriged map and the CT reconstruction.

RESULTS AND DISCUSSION

Five chamber experiments were conducted in this study. The time-averaged SF_6 concentrations at 31 sampling points in the measurement plane are shown in Figures 3a to 7a. The surface maps were produced from kriging the point sample data for easy visual comparison to the CT reconstructions (Figures 3b to 7b). The CT reconstructions of the simulation tests with the synthetic path integral concentrations calculated from the kriged surface maps for the same geometry to the experiment are also shown in Figures 3c–7c and Figures 3d–7d. The CT reconstructions from the experimentally measured path integral concentrations are shown in Figures 3e–7e using the ART algorithm and Figures 3f–7f using the PWLS method, respectively.

Point Sample Data and Kriged Maps

Point sample data were collected to compare with the CT reconstructions. However, there are several inherent

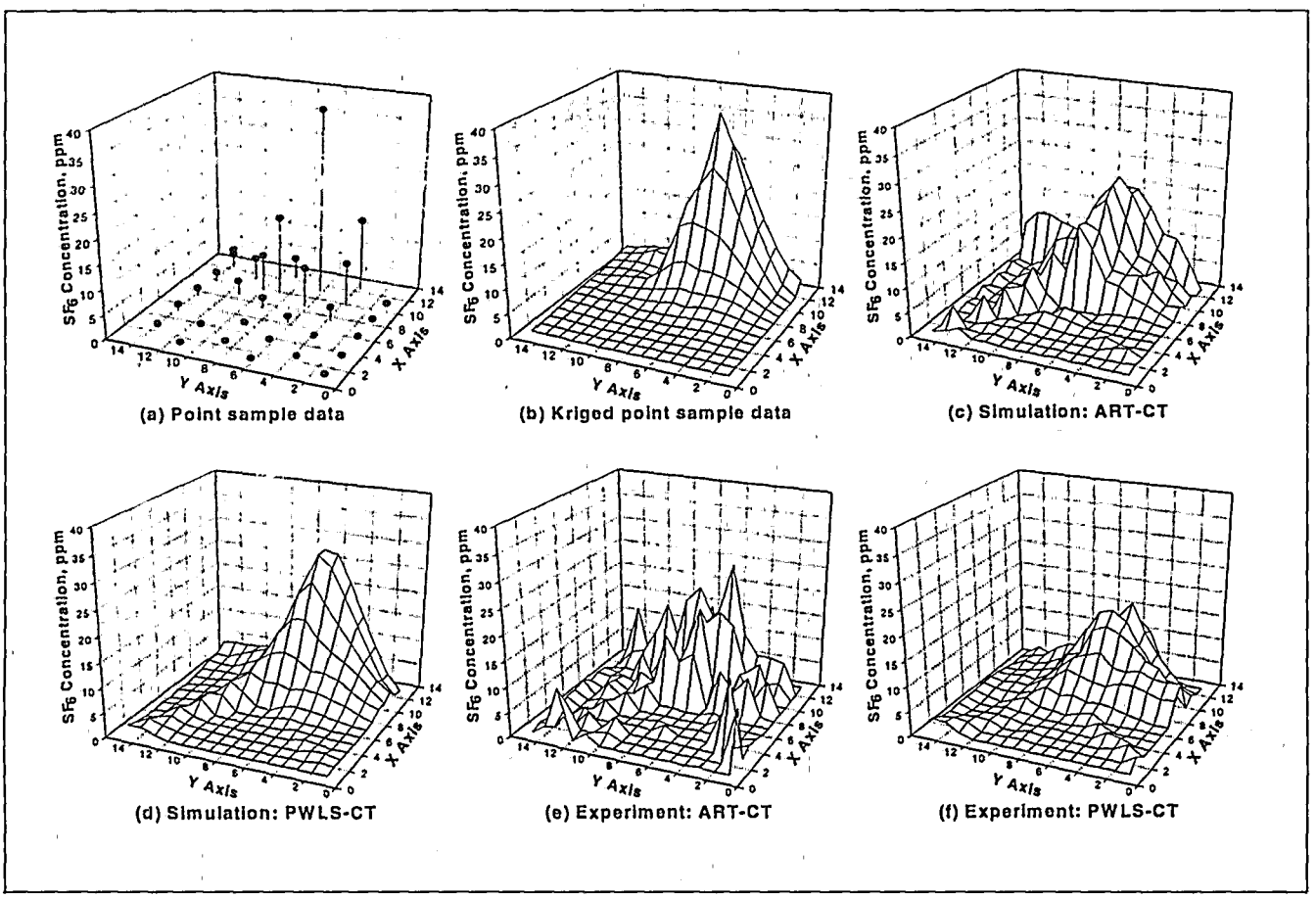

Figure 3. Point sample data and CT reconstructions with ART and PWLS methods in experiment 1: (a) Point sample data; (b) Kriged map from point sample data; (c) ART-CT reconstruction using experimental ray integrals; (d) PWLS-CT reconstruction using experimental ray integrals ($\beta = 2^{-3.3}$); (e) ART-CT reconstruction using simulated ray integrals from kriged map; and (f) PWLS-CT reconstruction using simulated ray integrals from kriged map ($\beta = 2^{-6.0}$).

limitations to using point sample data for evaluating the quality of the CT reconstructions. It is not possible to collect a sufficient number of point samples to provide enough information for the complete definition of a concentration gradient profile in a plane. Point sample data also represent only spot concentrations of sampling locations. However, path integral concentration data represent the average of a cylindrical beam path rather than a point or line. Therefore, it is not possible to completely match the measured concentration levels between these two measurements. These limitations should be kept in mind when comparing the point sample data with the CT reconstructions of the experimental path integral concentrations.

CT Reconstructions in Simulation

In addition to the CT reconstructions with the experimentally measured path integral concentrations, CT reconstructions were conducted with the use of the synthetic path integral concentrations for all experimentally obtained concentration gradients. The synthetic path integral concentrations were calculated from the kriged point sample data. Therefore, the kriged maps are true concentration profiles in the simulation tests. The detailed procedure for the simulation test of the CT reconstruction is described in the literature.[11] These simulation tests provide useful information for evaluation of the CT reconstruction methods and ray geometry because the synthetic path integral concentrations are noise-free data.

All CT reconstructions show a certain level of artifacts. It is primarily due to the ill-conditioned nature that the number of unknown pixel values exceeds that of known path integral concentrations. The path lengths of the folded rays were also longer than those of parallel geometries that have been evaluated in other studies. In addition, the number of projections was not sufficient to reconstruct the original image. These factors increase the possible number of CT reconstructions having "valid" solutions by ART without convergence to the true map. In fact, the σ_{ray} values were extremely low for the ART-CT reconstructions, although the σ_{pixel} values were relatively larger (Table 1). This implies that consistent solutions were achieved by the ART algorithm itself. However, the peak heights were reduced in most ART-CT reconstructions, and the location of peaks was also shifted in some ART-CT

Table 1. The σ_{ray} and σ_{pixel} values of the CT reconstructions (unitless).

	σ_{ray}[a]				σ_{pixel}[b]			
	Simulation Test		Experiment		Simulation Test		Experiment	
Experiment	ART	PWLS	ART	PWLS	ART	PWLS	ART	PWLS
1	<0.00001	0.00501	0.02268	0.0860	0.4201	0.1803	0.6708	0.4912
2	<0.00001	0.01387	0.00001	0.1030	0.4569	0.1967	0.8951	0.4616
3	0.01863	0.01485	<0.00001	0.0571	0.4377	0.2232	0.5971	0.4773
4	<0.00001	0.00583	<0.00001	0.1068	0.3248	0.1687	0.6181	0.4398
5	<0.00001	0.00600	<0.00001	0.0796	0.1926	0.1092	0.4520	0.3811

[a]The σ_{ray} value indicates the agreement between the ray integrals of the kriged point sample data and the ray integrals of the CT reconstructions in simulation tests. For experimental CT reconstructions, it indicates an agreement between the measured ray integrals and calculated ray integrals from the reconstruction. A lower value implies a better agreement; [b]The σ_{pixel} value indicates an agreement between the pixel values of the kriged point sample data and the pixel values of the CT reconstructions. For perfect agreement, σ_{pixel} is zero. A lower value implies a better agreement.

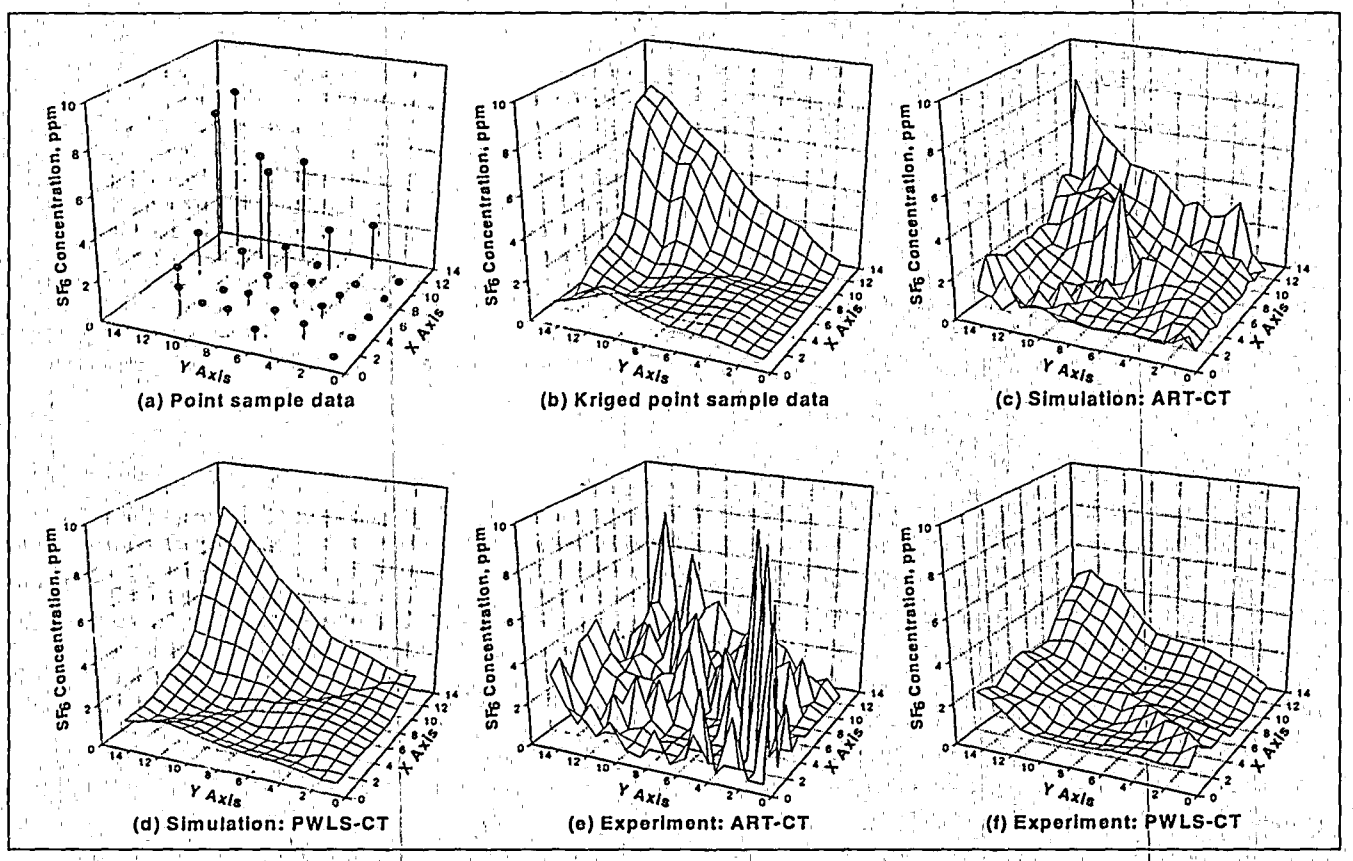

Figure 4. Point sample data and CT reconstructions with ART and PWLS methods in experiment 2: (a) Point sample data; (b) Kriged map from point sample data; (c) ART-CT reconstruction using experimental ray integrals; (d) PWLS-CT reconstruction using experimental ray integrals ($\beta = 2^{-1.8}$); (e) ART-CT reconstruction using simulated ray integrals from kriged map; and (f) PWLS-CT reconstruction using simulated ray integrals from kriged map ($\beta = 2^{-3.7}$).

reconstructions. In other words, ART could not converge to the true concentration profiles. Nevertheless, the algorithm found almost consistent solutions for the adjustment of pixel values to match the calculated path integral concentrations to the true path integral concentrations.

This problem can be remedied by increasing the number of projections and rays, as demonstrated in many previous published papers on simulation. In theoretical exercises, Todd et. al. have successfully produced fairly good CT reconstructions with relatively favorable ray geometries for concentration profiles having symmetrical Gaussian peaks.[3-6] However, they employed numerous virtual optical sources and detectors to create a number of intersected beam paths, which will not be feasible in any conceivable

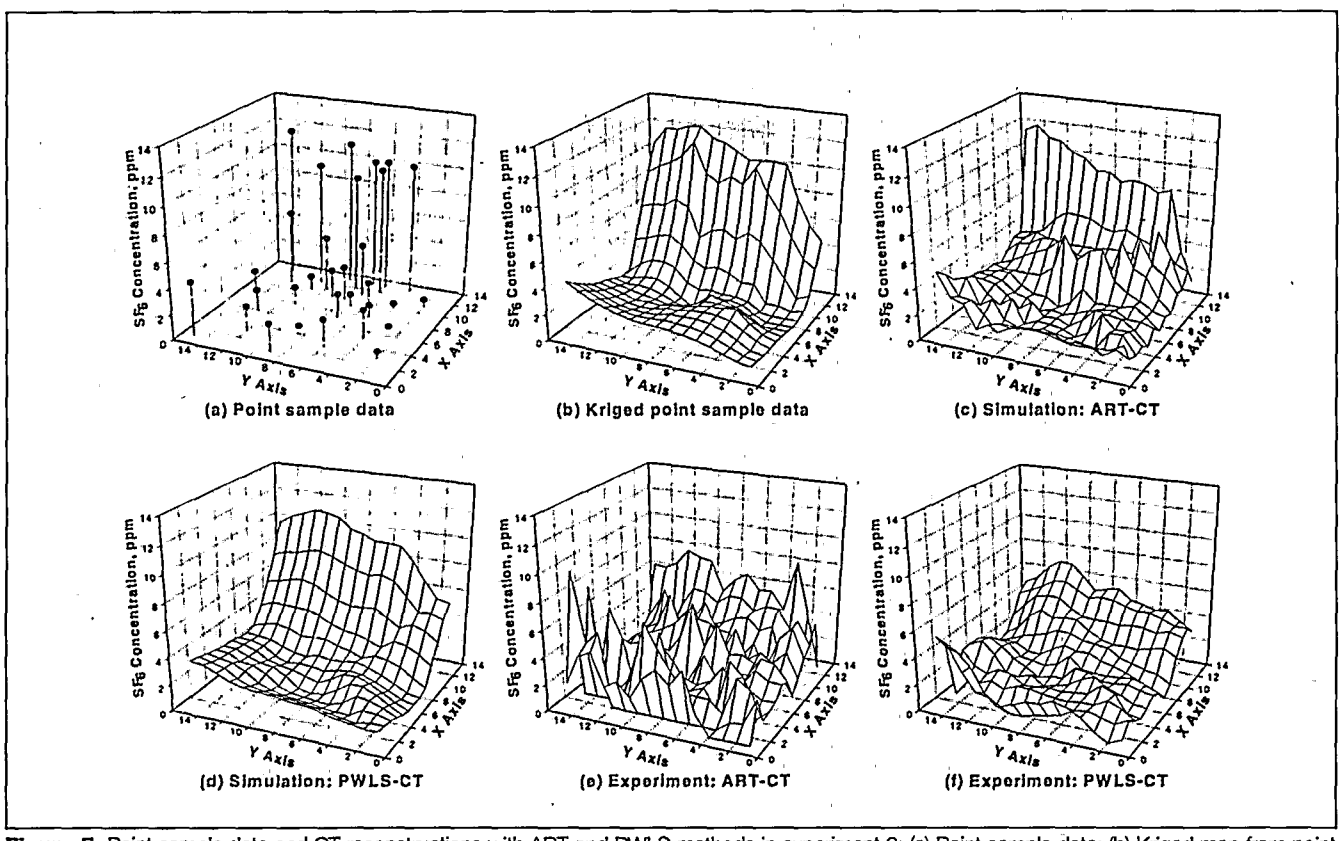

Figure 5. Point sample data and CT reconstructions with ART and PWLS methods in experiment 3: (a) Point sample data; (b) Kriged map from point sample data; (c) ART-CT reconstruction using experimental ray integrals; (d) PWLS-CT reconstruction using experimental ray integrals ($\beta = 2^{-3.1}$); (e) ART-CT reconstruction using simulated ray integrals from kriged map; and (f) PWLS-CT reconstruction using simulated ray integrals from kriged map ($\beta = 2^{-4.0}$).

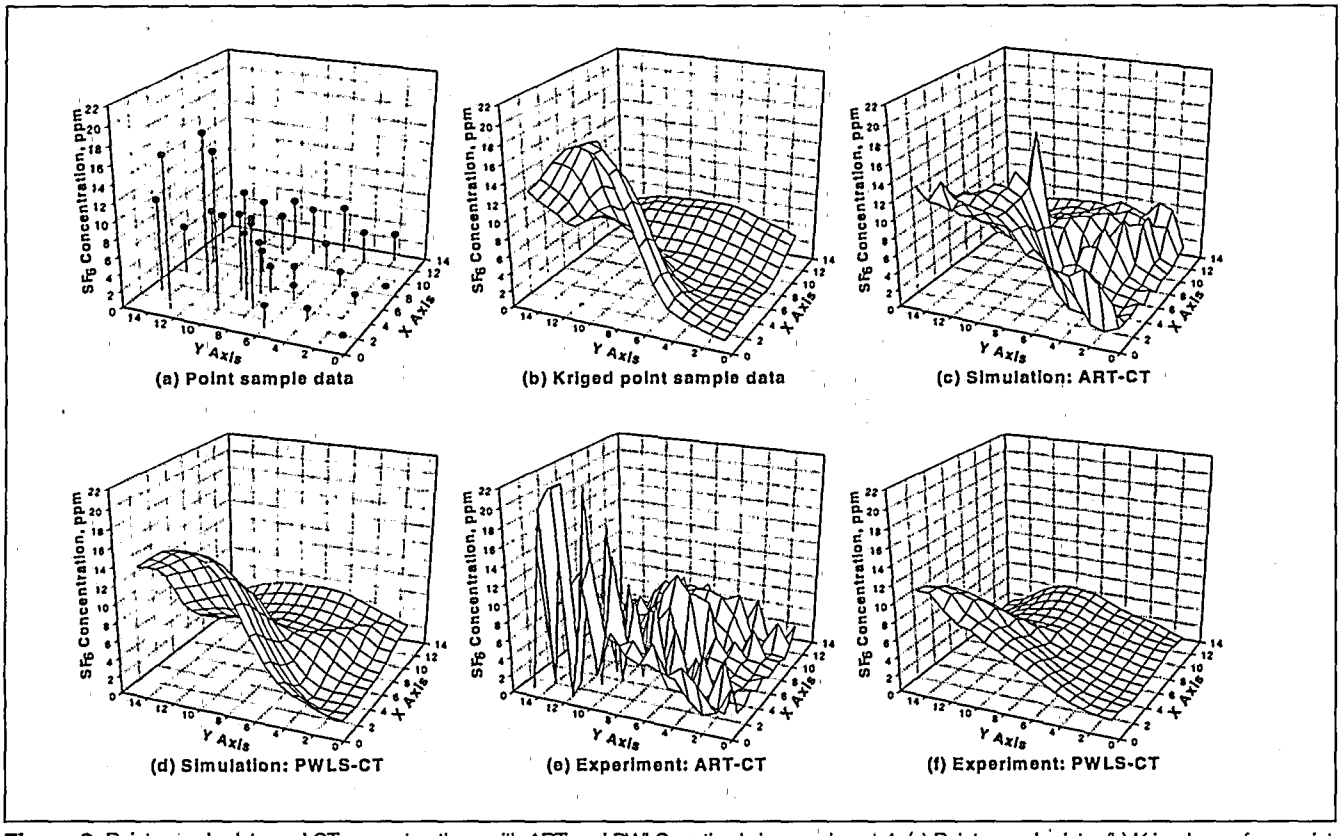

Figure 6. Point sample data and CT reconstructions with ART and PWLS methods in experiment 4: (a) Point sample data; (b) Kriged map from point sample data; (c) ART-CT reconstruction using experimental ray integrals; (d) PWLS-CT reconstruction using experimental ray integrals ($\beta = 2^{-0.1}$); (e) ART-CT reconstruction using simulated ray integrals from kriged map; and (f) PWLS-CT reconstruction using simulated ray integrals from kriged map ($\beta = 2^{-3.6}$).

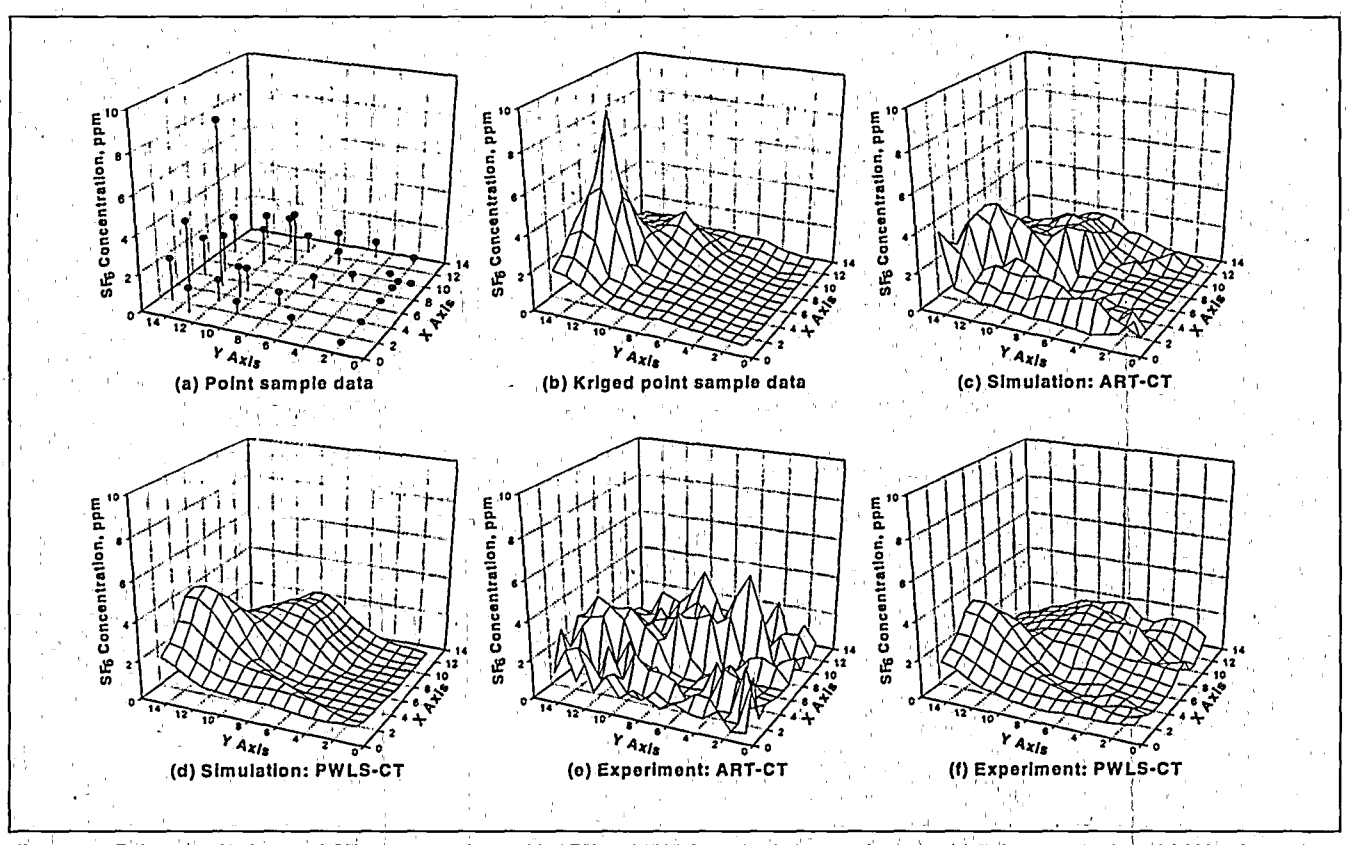

Figure 7. Point sample data and CT reconstructions with ART and PWLS methods in experiment 5: (a) Point sample data; (b) Kriged map from point sample data; (c) ART-CT reconstruction using experimental ray integrals; (d) PWLS-CT reconstruction using experimental ray integrals ($\beta = 2^{-1.9}$); (e) ART-CT reconstruction using simulated ray integrals from kriged map; and (f) PWLS-CT reconstruction using simulated ray integrals from kriged map ($\beta = 2^{-2.6}$).

field situation. Park et al. have also demonstrated that the quality of the CT reconstructions could be significantly improved by increasing the number of projections and rays even with the use of a single OP-FTIR.[11]

However, there is a tradeoff between these two. If the number of projections and rays is increased, the scanning time will be increased. Ideally, all path integral concentrations should be measured simultaneously to minimize inconsistency between the path integral concentrations. If scanning time is increased, inconsistency among the path integral concentrations will be increased because the time constants for features of the varying concentration field will be lower than those for the OP-FTIR measurement. That is, concentration patterns will continuously change during the scan. Therefore, it is desirable that the scanning time remains as short as possible. This factor was not considered in most previous simulation tests.[3-6]

No improvement of the CT reconstructions could be achieved by systematic modifications of the ART-CT reconstruction process, such as starting with different concentration maps for the first guess (zero, average, with some gradient randomly chosen), or by processing with different orders of path integral concentrations.

The most significant artifact of the ART-CT reconstructions was the appearance of unrealistically steep concentration gradients, as shown in Figures 3c to 7c. These irregular small peaks can be considered as an artifact shown in the simulation test results because air pollutant concentration gradients in the test maps (Figures 3b to 7b) have smoother patterns and no high, steep concentration gradients.

Noise, in the form of irregular small peaks, can be eliminated by post-filtering or post-smoothing as long as the CT reconstructions maintain the original concentration gradient patterns. Various regularization methods are generally used to remedy the irregular noisy peaks of the tomography reconstruction images.[16,17] However, these irregular peaks substantially deteriorate the CT reconstructions during CT processing. As the path integral concentrations were distributed to these small peaks, the true peaks could not be resolved effectively. Therefore, the reduction of the height of the main peaks, or concentration levels, in high concentration areas may be unavoidable. This is clearly shown in the case of experiment 1 (Figure 3c). There were no significant differences in the sums of pixel values between the kriged map and the ART-CT reconstructions with the synthetic path integral

concentrations. However, the peak heights were significantly reduced, and the peaks were broadened.

There is no definition or consensus of the phrase "complex concentration gradient" for CT reconstructions. However, in general, a "complex concentration gradient" can be said to be present when every pixel has a non-zero concentration value that is different than adjacent pixels. From this standpoint, all the experimentally obtained concentration patterns in this study could be considered to be both realistic and complex. Those artificially generated concentration patterns used in some previous studies, in contrast, have symmetrical Gaussian peaks on a zero-level background.[3-6] It was shown, in this simulation test, that the ART-CT reconstructions worked poorly for concentration profiles that were "complex."

The quality of the PWLS-CT reconstructions in the simulation tests was significantly improved compared to those of the ART-CT reconstructions. This is clearly demonstrated by the lower values of σ_{pixel} of the PWLS-CT reconstructions compared to those of the ART-CT reconstructions (Table 1). This is not surprising, since the PWLS algorithm was developed and optimized for PET scanning. PET scanning is exactly analogous to this situation, in which an underdetermined data set is used to generate concentration profiles for a rapidly changing concentration field. The improvement was maximized when concentration profiles had relatively low gradient patterns and broad peaks rather than steep and narrow peaks. PWLS successfully reproduced fairly good reconstructions, even for the highly complicated concentration gradient patterns, which have two peaks on the large smooth concentration gradient background over the entire pixels (Figures 5, 6, and 7). The most significant feature of the PWLS-CT reconstructions was that the small irregular noise peaks were almost completely eliminated. This improvement was expected from the fundamental nature of the PWLS algorithm. Therefore, the σ_{ray} values of the PWLS-CT reconstruction were actually higher than those of the ART-CT reconstructions in most experiments (Table 1). Again, this does not imply that the quality of the ART-CT reconstructions are better than the PWLS-CT reconstructions.

The CT reconstructions were conducted using the PWLS algorithm with various levels of β. The PWLS-CT reconstructions with a wide range of β values from 2^{-10} to 2^{10} were evaluated with use of the σ_{pixel} value. The relationships between the σ_{pixel} value and β values for experiments 1 and 3 are illustrated in Figure 8. The best agreements were achieved with β values in the range of $2^{-6} \sim 2^{-2}$ in most cases. The lowest β value ($\beta = 2^{-6.2}$) for the best reconstruction was found in the experimental reconstruction for experiment 1. These concentration patterns showed a single high narrow peak on the very low concentration background.

For concentration maps with lower gradients, the best fidelities were attained with higher β values. This trend was also expected because higher β values reduce concentration gradients between adjacent pixels. Thus, reproduction of higher peaks at higher gradients is inherently limited for high β values. However, it will not be simply corrected with use of a low β value, because the concentrations would be easily smeared into the irregular noise peaks that are increased with decrease of β value.

CT Reconstructions in Experiment

The CT reconstructions using both the ART and PWLS algorithms are shown in Figures 3e to 7e and Figures 3f to 7f, respectively. Clearly, ART failed to reconstruct the true

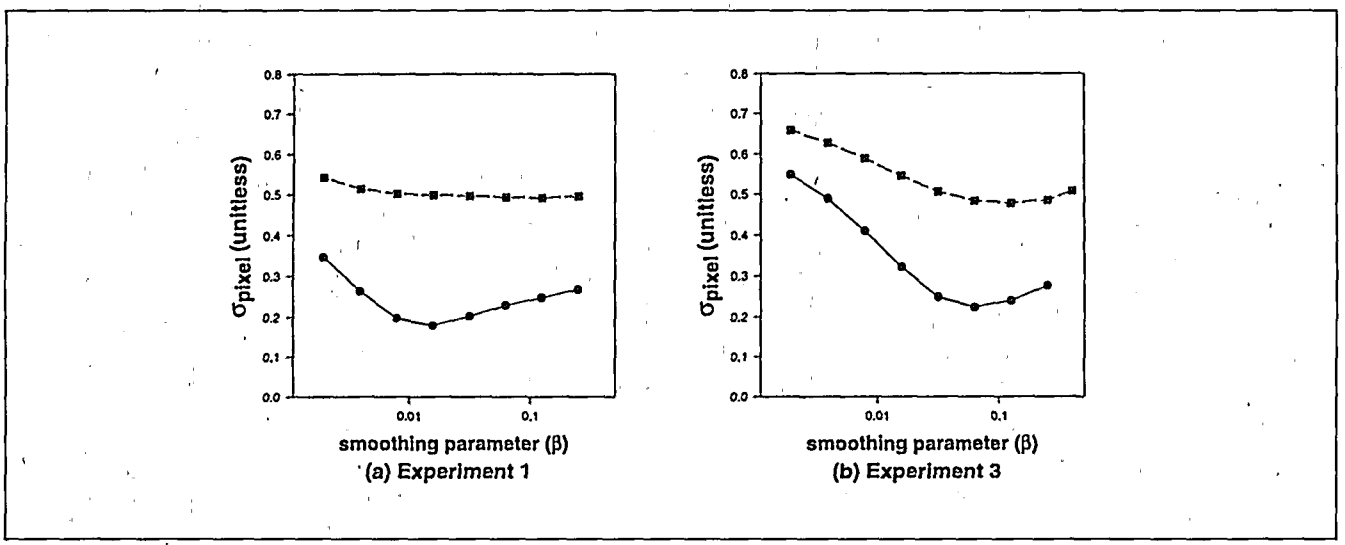

Figure 8. The σ_{pixel} values at various levels of smoothing parameter β for the PWLS-CT reconstruction with the synthetic ray integrals (•) and the experimentally measured ray integrals (■). The β values in each figure were shown when the lowest σ_{pixel} values were achieved.

concentration maps in most cases (although the true concentration profiles are actually unknown). First, highly fluctuating irregular concentration peaks were found in all ART reconstructions. Stationary ventilation conditions were maintained during the experiments, and only one or two steady sources were used for the experiment. Moreover, the ray data were averaged over the time period for about 1 hr. Therefore, air concentration profiles would be expected to have smooth gradient patterns rather than highly irregular, noisy concentration gradient patterns. Besides the irregular noise peaks, the ART reconstructions did not, in most cases, show similar concentration patterns to the kriged map from the point sample data.

The quality of the ART-CT reconstructions in the experimental study would be hardly improved by using any form of post-reconstruction regularization because the noise levels of the images generated by ART were too severe in most cases. For example, the ART-CT reconstructions in experiments 2–5 showed completely different concentration profiles from the kriged maps. Conclusively, ART reproduced extremely noisy images for those experiments with a simple narrow peak concentration gradient pattern and failed to reconstruct the original images properly for most other concentration profiles.

In general, the reconstructions by PWLS showed a fairly good agreement with the kriged maps in most experiments. Peak locations were correctly reproduced, and the general patterns of concentration gradients were fairly similar to those of the kriged point sample data, except for experiment 5. However, several differences between the kriged maps and the PWLS-CT reconstructions were observed. The most serious artifact was the notable reduction of peak height in every experiment. It may be possible to improve on the method by using a nonquadratic roughness penalty.

Again, there is a fundamental difference between the two images of the kriged point sample data and the CT reconstruction. The kriged maps from the point sample data represent a two-dimensional concentration map of a very thin slice of the measurement plane. However, the CT reconstructions represent a two-dimensional concentration map of the 20-cm-thick (beam width) plane. In addition, a certain level of error is inherently embedded into the two-dimensional concentration maps during the kriging process from the limited number of point sample data. Therefore, the measured path integral concentrations themselves will not necessarily match the path integral concentrations calculated from the kriged maps. In fact, the measured path integral concentrations were generally lower than those calculated from kriged maps (Table 2). The average level of the measured path integral concentrations was 86% of that of the path integral concentrations calculated from the kriged map. Thus, part of the reason for the reduction of the peak heights can be explained by this bias. However, it is believed that the measured path integral concentrations agree with those calculated from the kriged maps, considering the many differing factors between these two.

As the measured path integral concentrations essentially have a certain level of measurement errors, the optimum β values were increased for the best reconstructions compared to the simulation tests (Figure 8). The β values for the lowest value of σ_{pixel} ranged from $2^{-3.9} \sim 2^{2.6}$. These β values were much higher compared to those in the simulation tests which used the noise-free synthetic data. Therefore, the effect of the penalty terms in reducing the differences between neighboring pixel values was enlarged as the β values increased, which resulted in reduction of the peak heights.

For the experimental CT reconstructions, the σ_{ray} values using ART were lower than those using PWLS in the simulation tests. Despite the extremely low σ_{ray} values observed, ART apparently failed to reconstruct the original images in most cases, and the experimental path integral concentrations necessarily had a certain amount of measurement errors (see Table 1). Therefore, we concluded that there are many almost consistent but wrong solutions using ART with the experimental geometry due to the highly underdetermined system.

Because of the penalty function in the PWLS reconstruction process, this indeterminacy problem was less than in the ART-CT reconstructions. The σ_{ray} values of the CT reconstructions using PWLS were higher than those using ART. As various β values were applied, the variations of

Table 2. The sum of 56 ray integrals, in ppm-m^2.

Experiment	Kriged Map	Simulation Test ART	Simulation Test PWLS	Measured Ray[a]	Experiment ART	Experiment PWLS
1	767.3	767.3	767.5	665.0 (86.7)	668.5	663.0
2	305.2	305.2	305.4	318.4 (104.3)	318.4	315.1
3	655.1	655.1	655.7	560.7 (85.6)	560.7	557.6
4	1215.6	1215.6	1216.0	900.8 (74.1)	900.7	885.5
5	490.1	490.1	490.0	390.6 (80.0)	390.5	385.6

[a]Figures in ( ) indicate the percentage of the measured ray integrals to those calculated from the kriged map. Average of all experiments was 86.1 %.

the σ_{pixel} values were larger in experimental PWLS-CT reconstructions relative to the simulation tests, probably because the CT reconstructions were compared to the kriged map, which does not reflect the "true" concentration profiles.

Geometry Effects

The experimental geometry is fundamentally unsatisfactory, since it produces only 56 known variables (path integral concentrations) for the 195 unknowns (pixel values). The ratio of the number of pixels to the number of rays in this study was 3.5, and the number of projections was 4. Theoretically, the ratio of the number of pixels to the number of rays should be less than 1 for the perfect solution with a proper number of projection angles. However, this is not achievable in real environmental situations due to practical limitations.

The beam path lengths were longer in this study relative to those in other previous simulation studies.[3,5,6] In practice, it was necessary to make the path lengths longer to create multiple intersected beam paths with a single OP-FTIR scanning system. As the beam paths became longer, the indeterminacy increased. The scanning beam approach resulted in another unfavorable condition: beam paths were not evenly distributed over the whole plane.

Another problem in this geometry was found from the experimental ray measurement data. Figure 9 shows the average beam path concentration for all path integral concentrations in a well-mixed condition. Average beam path concentrations were expected to be about the same between neighboring rays because SF_6 was well mixed. For this test, SF_6 was released into the chamber for 2 min at an emission rate of 2 L/min, then the chamber was left with no mechanical ventilation. The path integral concentrations were continuously measured after mixing started. Figure 9 shows the beam path average concentrations of each ray which were measured 43–49 min after mixing started. Ray numbers 12, 13, 27, 28, 40, and 41 showed higher concentration levels and were not consistent with the average concentration of the room or with the adjacent rays. These data were relatively constant during the full period of this experiment. Therefore, it was believed that the measurement for these ray numbers were biased. All these rays were assumed to have short path lengths, which traveled only from the FTIR to the flat mirrors or retroreflectors and back to the FTIR. It was assumed that the cause of this bias was misalignment rather than the characteristics of the beam path (such as the beam divergence) because these erroneous high concentrations were not observed in ray numbers 55 and 56, which had quite similar configurations.

These discrepancies could be explained due to misalignment of the beam path. These IR beams might have traveled to the opposite retroreflectors due to misalignment of the flat mirrors and the characteristics of retroreflectors. However, this bias could not be corrected for the CT reconstructions because the fine adjustments of the flat mirrors and retroreflectors were conducted for every experiment for the best IR beam collection. It was impossible to identify the error levels for path integral concentrations with the concentration gradient profiles. Once the possible error sources are identified, they can be easily corrected. This type of error can be eliminated by blocking the outside of the IR beam source, or by correction of alignments for all beams. This is, in practice, a non-trivial issue.

CONCLUSION

Five full room-sized chamber experiments were successfully completed in this study of CT reconstructions using both the ART and PWLS algorithms. The beam geometry was highly underdetermined in terms of both the number of rays and projections. This beam geometry was chosen because it could generate a number of intersected beam paths with the use of a single OP-FTIR scanning system, 52 flat mirrors, and four retroreflectors.

ART could not converge to the original images for most measured concentration profiles. However, the agreement of path integral concentrations between true and calculated ones from the CT reconstruction was achieved

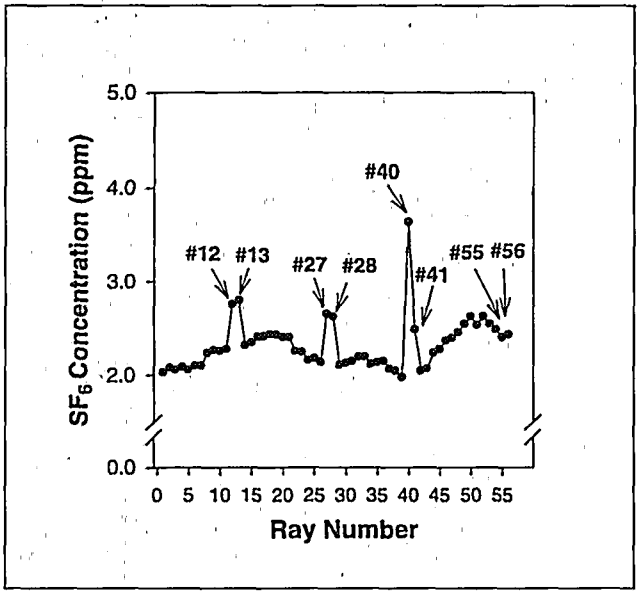

Figure 9. Average concentration of each path integral in the well-mixed condition. The average concentration of each ray integral was expected not to differ greatly between adjacent rays because the tracer was well mixed for 43 min after releasing SF_6 for 2 min at an emission rate of 2 L/min. Path integral data were collected in series between 43 and 49 min. Ray numbers 12, 27, 40, and 55 are the short rays, which were aligned to be reflected from the flat mirrors to the OP-FTIR directly. Ray numbers 13, 28, 41, and 56 are the short rays to the retroreflectors that were reflected to the OP-FTIR directly. High concentration levels are assumed to have been caused by misalignment.

nearly perfectly. This implies that while ART can match the path integral concentrations, it cannot reconstruct the original images under highly underdetermined conditions with this ray geometry. The CT reconstructions were significantly improved by PWLS, which is structured to encourage agreement between the path integral concentrations and to discourage disparities among neighboring pixels. The general concentration gradient patterns were successfully reproduced. The peak locations were correctly positioned in the PWLS-CT reconstructions. A notable feature of the PWLS-CT reconstructions was a significant reduction of highly irregular noise peaks found in the ART-CT reconstructions. However, the peak heights were reduced in the PWLS-CT reconstructions due to the nature of the PWLS algorithm.

For the best agreement with the kriged maps, β, which balances the tradeoff between the two conflicting goals in the PWLS algorithm, was shown to fall in the range of 2^{-6} to 2^{-2} in the simulation tests and $2^{-3.9}$ to $2^{2.6}$ in the experimental CT reconstructions. Although minor artifacts were observed, PWLS could successfully generate CT reconstructions in terms of peak locations and the concentration gradient patterns.

ACKNOWLEDGMENTS

The authors would like to thank Zhou Yi, Jyunde Wu, Anushka Drescher, and Robert Spear at the University of California at Berkeley for assistance with the experiment. The authors also thank ETG Inc. for technical support. This study was supported by NIOSH grant 1R01-OH02666.

REFERENCES

1. Wolfe, D.C. On the Application of Optical Computed Tomography to Remote Air Pollution Measurements. Ph.D. Dissertation, Stanford University, Palo Alto, CA,1980.
2. Bennett, K.E.; Faries, G.W.; Byer, R.L. "Experimental optical fan beam tomography," *Appl. Opt.* 1984, *23(18)*, 2678.
3. Todd, L.; Leith, D. "Remote sensing and computed tomography in industrial hygiene," *Am. Ind. Hyg. Assoc. J.* 1990, *51(4)*, 224.
4. Ramachandran, G.; Leith, D.; Todd, L. "Extraction of spatial aerosol distributions from multispectral light extinction measurements using computed tomography," *J. Opt. Soc.* 1993, *11(1)*, 144.
5. Todd, L.; Ramachandran, G. "Evaluation of optical source-detector configurations for tomographic reconstruction of chemical concentrations in indoor air," *Am. Ind. Hyg. Assoc. J.* 1994, *55(12)*, 1133.
6. Todd, L.; Ramachandran, G. "Evaluation of algorithms for tomographic reconstruction of chemical concentrations in indoor air," *Am. Ind. Hyg. Assoc. J.* 1994, *55(5)*, 403.
7. Park, D.Y.; Levine S.L.; Russwurm, G.M. Fourier Transform Infrared Optical Remote Sensing; In *Encyclopedia of Environmental Analysis and Remediation*; John Wiley & Sons, Inc.: New York, 1998; Vol. 7, pp 4137-4149.
8. Yost, M.G.; Gadgil, A.J.; Drescher, A.C.; Zhou, Y.; Sigmond, M.A.; Levine, S.P.; Nazaroff, W.W.; Saisan, P.A. "Imaging indoor tracer-gas concentrations with computed tomography: Experimental results with a remote sensing FTIR system," *Am. Ind. Hyg. Assoc. J.* 1994, *55(5)*, 395.
9. Drescher, A.C.; Park, D.Y.; Yost, M.G.; Gadgil, A.J.; Levine, S.P.; Nazaroff, W.W. "Chamber studies of trace gas concentration measurements using open path FTIR remote sensing and SBFM computed tomography," *Atmos. Environ.* 1997, *31(5)*, 727.
10. Drescher, A.C.; Gadgil, A.J.; Price, P.N.; Nazaroff, W.W. "Novel approach for tomographic reconstruction of gas concentration distributions in air: Use of smooth basis functions and simulated annealing," *Atmos. Environ.* 1996, *30(4)*, 929.
11. Park, D.Y.; Yost, M.G.; Drescher, A.C.; Levine, S.P. "Evaluation of virtual source beam configurations for rapid tomographic reconstruction of gas and vapor concentrations in workplaces," *J. Air & Waste Manage. Assoc.* 1997, *47*, 582.
12. Fessler, J A. ASPIRE 3.0 User's Guide: A Sparse, Precomputed, Iterative Reconstruction Library; Technical Report 293; Communications and Signal Process Lab, Department of Electrical Engineering and Computer Science, University of Michigan: Ann Arbor, MI, 1995.
13. Fessler, J.A. "Penalized weighted least-squares image reconstruction for positron emission tomography," *IEEE Trans. Medical Imaging* 1994, *13(2)*, 290.
14. Jones, T.A.; Hamilton, D.E.; Johnson, C.R. *Contouring Geologic Surfaces with the Computer*; Van Nostrand Reinhold: New York, 1986.
15. Brooks, R.A.; Di Chiro, G. "The theory of image reconstruction in computed tomography," *Radiology* 1975, *117*, 561.
16. Hanson, K.M. Noise and Contrast Discrimination in Computed Tomography. In *Radiology of the Skull and Brain*, Vol. 5, Technical Aspects of Computed Tomography; Newton, T.H.; Potts, D.G., Eds.; C.V. Mosby: St. Louis, MO, 1981; ch. 113, pp 3941-3955.
17. Ledley, R.S. "Introduction to computed tomography," *Comput. Biol. Med.* 1976, *6(4)*, 239.

About the Authors

Doo Y. Park, corresponding author, is assistant professor of industrial health at the Hansung University. He is a committee member of Optical Remote Sensing at the U.S. Naval Air Facility in Atsugu, Japan. He received his Ph.D. from the University of Michigan and his M.P.H. from Seoul National University. His address is Department of Industrial Safety Engineering, Hansung University, 389-2 Samsun-dong, Sungbuk-ku, Seoul, 136-792 Korea; e-mail: dooyong@hansung.ac.kr.

Jeffery A. Fessler is an assistant professor in the Department of Electrical Engineering and Computer Science, with secondary appointments in the Departments of Biomedical Engineering and the Division of Nuclear Medicine. His address is 4240 EECS Bldg., 1301 Beal Ave., Ann Arbor, MI, 48109-2122; email: fessler@umich.edu.

Michael G. Yost is associate professor of environmental health, School of Public Health, University of Washington, and co-principal investigator of NIOSH Grant R01-OH02666. His address is Department of Environmental Health, University of Washington, Seattle, WA 98195; e-mail: airion@u.washington.edu.

Steven P. Levine is professor of occupational and environmental health, and director of NIOSH Grant R01-OH02666. His address is: Department of Environmental and Industrial Health, School of Public Health, University of Michigan, Ann Arbor, MI 48109-2029; e-mail: SLIH@umich.edu.